PNAS RESEARCH ARTICLE | EARTH, ATMOSPHERIC, AND PLANETARY SCIENCES

Tropical Andean climate variations since the last deglaciation

Boyang Zhao (赵伯阳)[a,1], James M. Russell[a], Ansis Blaus[b], Majoi de Novaes Nascimento[c], Aaron Freeman[a], and Mark B. Bush[b]

Affiliations are included on p. 6.

Edited by Eric Rignot, University of California Irvine, Irvine, CA; received November 21, 2023; accepted June 7, 2024

Global warming during the Last Glacial Termination was interrupted by millennial-scale cool intervals such as the Younger Dryas and the Antarctic Cold Reversal (ACR). Although these events are well characterized at high latitudes, their impacts at low latitudes are less well known. We present high-resolution temperature and hydroclimate records from the tropical Andes spanning the past ~16,800 y using organic geochemical proxies applied to a sediment core from Laguna Llaviucu, Ecuador. Our hydroclimate record aligns with records from the western Amazon and eastern and central Andes and indicates a dominant long-term influence of changing austral summer insolation on the intensity of the South American Summer Monsoon. Our temperature record indicates a ~4 °C warming during the glacial termination, stable temperatures in the early to mid-Holocene, and slight, gradual warming since ~6,000 y ago. Importantly, we observe a ~1.5 °C cold reversal coincident with the ACR. These data document a temperature change pattern during the deglaciation in the tropical Andes that resembles temperatures at high southern latitudes, which are thought to be controlled by radiative forcing from atmospheric greenhouse gases and changes in ocean heat transport by the Atlantic meridional overturning circulation.

paleoclimate | tropical South America | temperature | branched GDGT | lake sediments

Significance

Tropical South America is a center of biodiversity and is under pressure from ongoing climate change. Understanding tropical South America's climate history can provide valuable insight into the water cycle, ecosystems, and future climate change, yet past temperature changes are not well-known. We reconstructed temperature and rainfall since ~16,800 y ago in the tropical Andes Mountains. In addition to warming driven by rising atmospheric CO_2 concentrations, we observe rapid temperature changes linked to changes in the deep ocean circulation. Given the projected slowing of the Atlantic Ocean circulation in the coming decades, our findings suggest that Amazonia's ecosystems may be challenged by rapid temperature changes superposed on warming from sharply increasing atmospheric CO_2.

The last glacial termination (T1, 21 to 11.6 thousands of calibrated radiocarbon years B.P., hereafter k cal BP) is the most recent period during which global warming was associated with increasing atmospheric greenhouse gas concentrations (GHGs) (1, 2). Global warming during T1 was interrupted by millennial-scale episodes of cooling such as the Younger Dryas (YD) and Antarctic Cold Reversal (ACR). Whereas warming during T1 was ubiquitous, due in part to global radiative forcing by GHGs (2), millennial-scale cooling events, including the YD and ACR, are antiphase between the hemispheres (3). There are several hypotheses for the causes of these events (4); however, marine sedimentary $^{231}Pa/^{230}Th$ ratios show that intervals of northern hemisphere cooling, such as the YD, are associated with diminished northward heat transport by the Atlantic Meridional Overturning Circulation (AMOC) (5), and climate data-model syntheses support the importance of AMOC variations to hemispherically antiphase temperature changes (2, 6). Although northern high-latitude cooling during the YD and southern high-latitude cooling during the ACR are well known, millennial-scale temperature variations in the tropics are less well characterized. Geochemical records from eastern African lakes vary, with some records suggesting cooling during the YD (7, 8), some showing cooling during the ACR (9), and others suggesting little coherent millennial-scale variability (10), and the spatiotemporal pattern of temperature change in the tropical Andes is debated (11–17). It is important to understand the tropical temperature response to climate forcings in the past in light of ongoing climate warming and the potential for disruptions to polar temperatures and AMOC in the coming decades.

Glacial geologic records, fossil pollen, and ground water noble gases have provided valuable insight into tropical South America's (TSA) temperature history (18–22). These records suggest temperatures warmed by ~4 to ~7 °C during T1, and glacial geologic records from the tropical Andes suggest expanded glaciers during the ACR (11). Recent syntheses of records from the Bolivian Andes suggest ACR cooling, but have relatively few dated moraines between 14.5 and 12.9 ka (16). Some glacial geologic records suggest heterogeneous temperature changes in TSA during the YD (11, 13–17, 23). The precision and accuracy of cosmogenic production rates in the High Andes has improved in the last decade, yet the uncertainties in cosmogenic radionuclide exposure ages can still be ~5% of the age itself, challenging our ability to link glacial landforms to abrupt, millennial to submillennial climate events (24–30). Resolving these issues could elucidate the impacts of high latitude cooling on tropical land temperatures, and the coupling between long-term changes in temperature, the water cycle, and tropical landscapes.

Author contributions: B.Z. and J.M.R. designed research; B.Z., J.M.R., A.B., M.d.N.N., A.F., and M.B.B. performed research; A.B., M.d.N.N., and M.B.B. contributed new reagents/analytic tools; B.Z., J.M.R., and M.d.N.N. analyzed data; and B.Z., J.M.R., A.B., M.d.N.N., A.F., and M.B.B. wrote the paper.

The authors declare no competing interest.

This article is a PNAS Direct Submission.

Although PNAS asks authors to adhere to United Nations naming conventions for maps (https://www.un.org/geospatial/mapsgeo), our policy is to publish maps as provided by the authors.

Copyright © 2024 the Author(s). Published by PNAS. This article is distributed under Creative Commons Attribution-NonCommercial-NoDerivatives License 4.0 (CC BY-NC-ND).

[1]To whom correspondence may be addressed. Email: boyang_zhao@brown.edu.

This article contains supporting information online at https://www.pnas.org/lookup/suppl/doi:10.1073/pnas.2320143121/-/DCSupplemental.

Published August 12, 2024.

Downloaded from https://www.pnas.org by "BROWN UNIVERSITY , ROCKEFELLER LIBRARY" on May 23, 2025 from IP address 128.148.194.11.

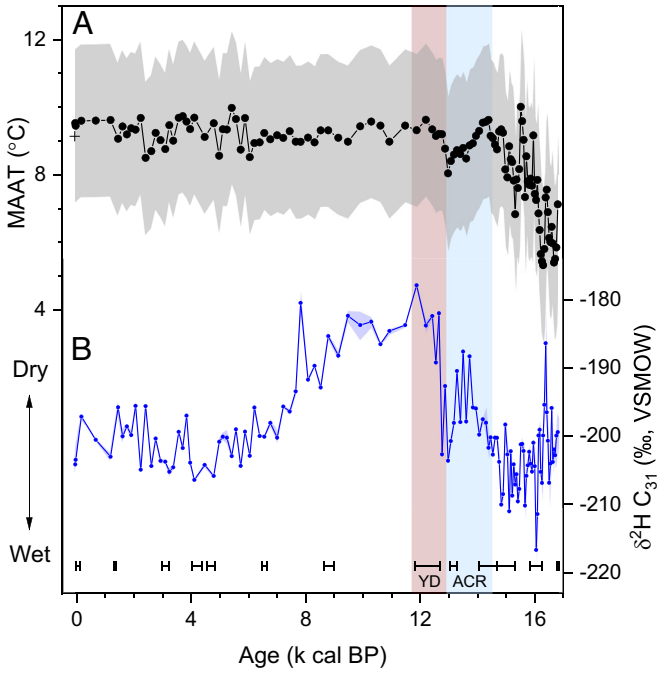

Fig. 1. Reconstructions of temperature (*A*) and hydroclimate (*B*) from Laguna Llaviucu over the past ~16.8 k cal BP. The plus symbol denotes the modern temperature observation of 9.14 °C from the Laguna Llaviucu region (39). An error bar of ±2.26 °C from the calibration (33) is shown with the gray shading in (*A*). Blue shading in (*B*) denotes 1 σ measurement uncertainty. The range symbols hovering above *x* axis represent the radiocarbon dating constraints. YD, Younger Dryas. ACR, Antarctic Cold Reversal.

It has traditionally been difficult to reconstruct tropical terrestrial temperatures due to the discontinuous nature of glacial geologic records and a lack of other temperature-sensitive proxies. Recently, branched glycerol dialkyl glycerol tetraethers (brGDGTs) have emerged as a new tool for paleotemperature reconstruction (31–33). Here, using brGDGTs and leaf wax hydrogen isotopes (δ^2H) in a sediment core, we report paired temperature and hydroclimate records of the past ~16.8 k cal BP from Laguna Llaviucu (*SI Appendix*, Fig. S1). This moraine-dammed lake lies at 3,152 m above sea level, and the Llaviucu valley supports a wet montane forest on the Eastern Cordillera of the Ecuadorian Andes.

Orbital-Scale Tropical Andean Precipitation Is Dominated by Austral Summer Solar Insolation Forcing

Hydrogen isotopes of leaf waxes from lake sediments have been widely used to investigate variations in the amount of precipitation through time under the assumption that ^2H-depleted waxes are associated with intensified precipitation vis-á-vis the amount effect (34–36). Modern observation from the Andes and Amazon found that the hydrogen isotopes in plant *n*-alkanes and source water are correlated, supporting the use of hydrogen isotopes of *n*-alkanes to reconstruct hydroclimate (37). Although moisture source and other factors may affect precipitation ^2H values (38), monthly precipitation amounts and ^2H values in this region are significantly negatively correlated (*SI Appendix*, Fig. S2), as predicted by the amount effect.

We produced δ^2H of C_{31} alkanes preserved in a well-dated sediment core (*SI Appendix*, Fig. S3) from Laguna Llaviucu to examine the hydroclimate history of this location for the past ~16.8 k cal BP (Fig. 1 and *SI Appendix*, Fig. S4). As might be expected at this elevation and in such a wet setting, the $\delta^{13}C$ of C_{31} alkanes in our record is invariant (–32.5 ± 0.3‰, n = 25). This indicates that the vegetation near the lake was consistently dominated by plants using the C3 photosynthetic pathway; thus, the impact of changes in vegetation type (C3 vs. C4) on the isotopic fractionation between precipitation and the C_{31} alkanes in our record is minimal (*SI Appendix*, Fig. S5).

We observe ^2H-depleted waxes during the late Pleistocene and mid to late-Holocene, and ^2H-enriched waxes during the early Holocene, as well as multicentennial intervals of ^2H-enrichment and depletion during the ACR and near the start of the YD, respectively (Fig. 1). Our δ^2H record is strikingly similar to a $\delta^{18}O$ record from Santiago cave, located in the lowland forests ~110 km east of Laguna Llaviucu (Fig. 2). These records are strongly correlated despite the different paleoclimate archives, dating methods, and mechanisms by which precipitation isotopes are incorporated into leaf waxes and speleothem carbonate, indicating both sites experience similar hydroclimate fluctuations, receive the same source water (in light of Santiago's location, likely the Atlantic) since the deglaciation, and demonstrates that our age control and the timing of millennial variations recorded in Laguna Llaviucu sediments are robust.

At the orbital scale, our records indicate drying during the deglaciation, dry conditions during the early Holocene, and a transition toward wetter conditions from ~10 to 6 k cal BP (Figs. 1 and 2). This pattern tracks variations in austral summer insolation in the southern tropics (41), in keeping with predictions that the South American summer monsoon (SASM) is strongly influenced by austral summer insolation on precession timescales (42–44). At the millennial scale, our record suggests dry conditions during the beginning of the ACR, a brief wet interval at the end of the ACR/start of the YD, and rapid drying near the onset of the YD. These patterns differ somewhat from records further to the north and south, where, for instance, drought in the northern TSA and wet conditions in southern TSA during the YD reflects shifts in the strength of the SASM associated with North Atlantic cooling and changes in the interhemispheric thermal gradient (16, 34, 43–48). The multicentennial wet interval at the end of the ACR and start of the YD rainfall does not precisely align with the patterns of change observed to the north and south, and could reflect the equatorial location of our record and the migration of the Intertropical Convergence Zone (ITCZ) from north to south as North Atlantic temperatures cooled (*SI Appendix*, Fig. S6). The mid-to-late Holocene transition from dry to wet also aligns with an increase in rainfall interpreted to reflect intensified El Nino-Southern Oscillation (ENSO) in nearby Laguna Pallcacocha (49–52). We speculate that the strong multicentennial variability in the late Holocene in our record could be associated with intensified ENSO (53), but note that our records' resolution is too low to document ENSO variability, particularly given the complexity of ENSO reconstruction in this region (54, 55).

Cooling during the Antarctic Cold Reversal in the Tropical Andes. brGDGTs are a suite of bacterial membrane lipids that have been used to reconstruct terrestrial temperatures in Africa and Southeast Asia (56, 57). brGDGTs have not been previously used to reconstruct temperature in TSA, but recent calibration work validated and improved lacustrine brGDGT proxy calibrations to mean annual air temperature (MAAT) in TSA (33). We used the MBT'_{5ME} (methylation of branched tetraethers) index as a temperature proxy to reconstruct tropical Andean temperature history since ~16.8 k cal BP (Fig. 1). Our temperature reconstruction indicates a rapid ~4 °C warming from ~16.8 to 14.5 k cal BP. Prior

Downloaded from https://www.pnas.org by "BROWN UNIVERSITY , ROCKEFELLER LIBRARY" on May 23, 2025 from IP address 128.148.194.11.

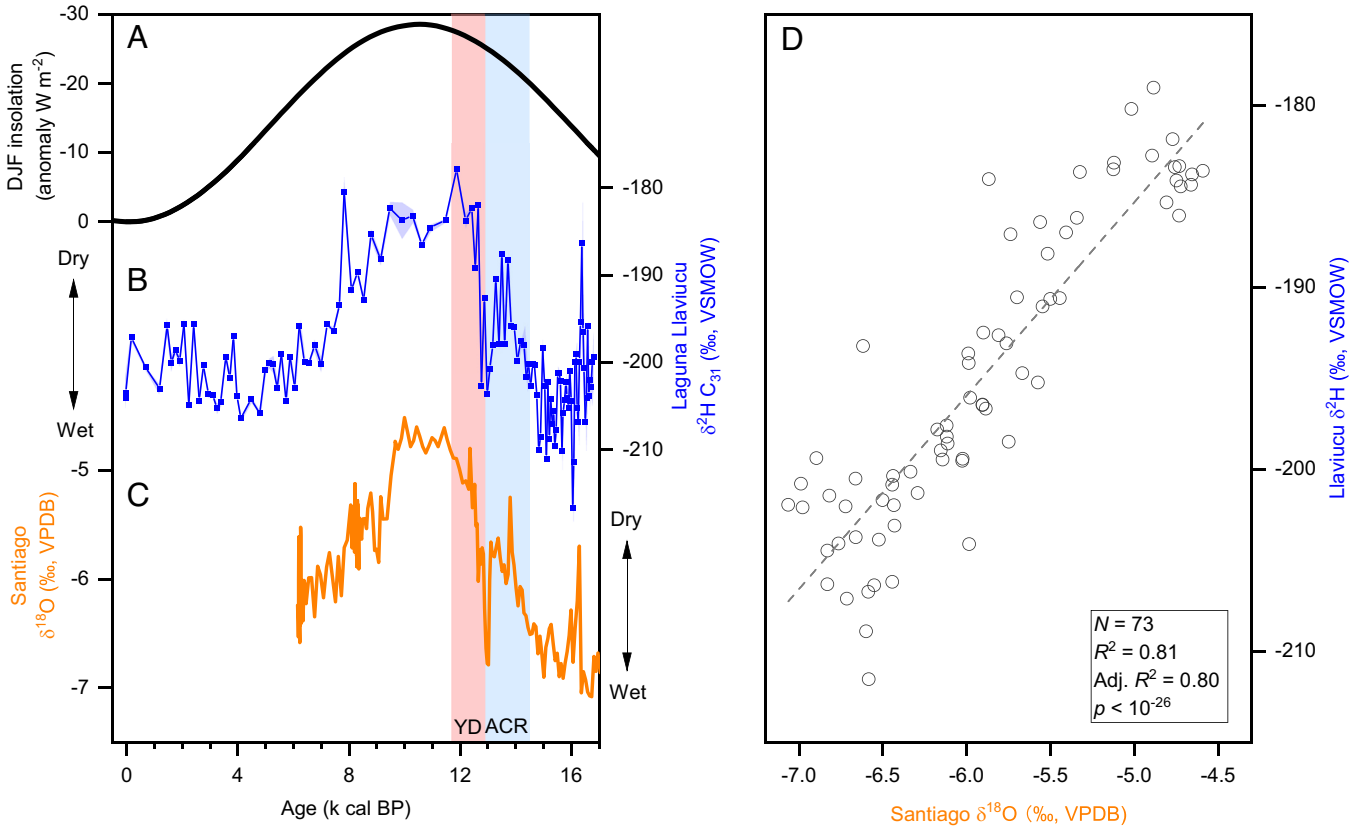

Fig. 2. Austral summer insolation (*A*) driving similar TSA hydroclimate variations from Laguna Llaviucu (*B*) and Santiago cave (40) (*C*), situated at high and low elevations, respectively. (*D*) Correlation between Llaviucu hydrogen isotopes and Santiago stalagmite oxygen isotopes. Blue shading in (*B*) denotes 1 σ measurement uncertainty. YD, Younger Dryas. ACR, Antarctic Cold Reversal.

paleotemperature estimates based on fossil pollen analysis suggest about 2 to 3 °C warming between the Last Glacial Maximum (LGM) at 22 k cal BP and 16 k cal BP, followed by 3 to 5 °C warming from 16 k cal BP to the Holocene (21, 58). Thus our reconstruction is consistent with a 5 to 7 °C warming since the LGM (21, 58). Our data, however, reveal that warming during T1 was not steady, with a ~1.5 °C cooling beginning at ~14.4 k cal BP that is coincident with the ACR recorded in Antarctic ice cores (59, 60) (Fig. 3). This event was followed by warming beginning at ~12.9 k cal BP, the start of YD, when the North Atlantic cooled and the AMOC weakened (5) (Fig. 3). Temperatures during the early Holocene are relatively stable, with a slight warming trend since ~6 k cal BP (~0.04 °C/kyr).

Jomelli et al. used cosmogenic radionuclide exposure ages to show that glaciers in both the northern and southern tropical Andes expanded during the ACR, with moraines marking the largest expansions dated to ~14.0 ka (11). Reconstructions from the Bolivian Andes support this finding, with moraines suggesting ACR-cooling of 4 °C dated to ~13.5 ka (16). Younger moraine ages about the time of the YD differ in timing in the northern and southern tropical Andes. This is hypothesized to reflect the retreat of southern tropical glaciers due to GHG-driven warming and the retreat of northern tropical glaciers due to warming caused by drought and vegetation feedbacks when the ITCZ migrated southward during the YD (11).

The timing of glacial advances during the ACR, between 14.0 and 13.5 ka (11, 16), occurs near the start of the cooling we observe at Laguna Llaviucu. The next youngest southern tropical Andean moraines date to ~12.1 ka, well after temperatures at Llaviucu warmed. As glacial moraine ages generally record the latter stages of boulder accumulation and the timing of the onset of glacier retreat, we might expect the largest advances to date to the end of the ACR at 12.9 k cal BP when temperatures at Llaviucu were coolest. These offsets could reflect uncertainty in the moraine ages or the influence of factors other than temperature on the glaciers that formed the moraines. Our record suggests that, at least in the region near Laguna Llaviucu, cooling from 14.5 to 13.5 k cal BP was accompanied by drying, the end of the ACR was relatively wet, and decreasing precipitation during the YD corresponded to a rapid rise in temperatures (Fig. 1). These results suggest an inconsistent relationship between temperature and precipitation during the last deglaciation in this region. Nevertheless, our data broadly support inferences that tropical Andean glaciers advanced or experienced standstills in the context of cooling during the ACR (11, 16).

Our reconstructed temperatures generally track EPICA Dome C hydrogen isotope records, with a notable ACR event and a slight warming trend since the middle Holocene (Fig. 3). CO_2 concentrations (pCO_2) are considered to be the main driver for Antarctic temperatures as well as global temperature change since the deglaciation (2, 64), and our results indicate that tropical Andean temperature variations were also influenced by pCO_2 changes on both millennial and orbital timescales. The pattern of temperature change in our reconstruction, Antarctic ice cores, and records of mean global ocean temperatures (MOT) imply strong connections between tropical land temperature, ocean temperatures, and the global energy balance that is best explained by atmospheric pCO_2 variations (62).

Millennial-scale temperature changes in the high latitudes during the last deglaciation are generally thought to stem from changes in freshwater discharge to the North Atlantic, which disrupt the AMOC and transport of heat to the north, causing

Downloaded from https://www.pnas.org by "BROWN UNIVERSITY , ROCKEFELLER LIBRARY" on May 23, 2025 from IP address 128.148.194.11.

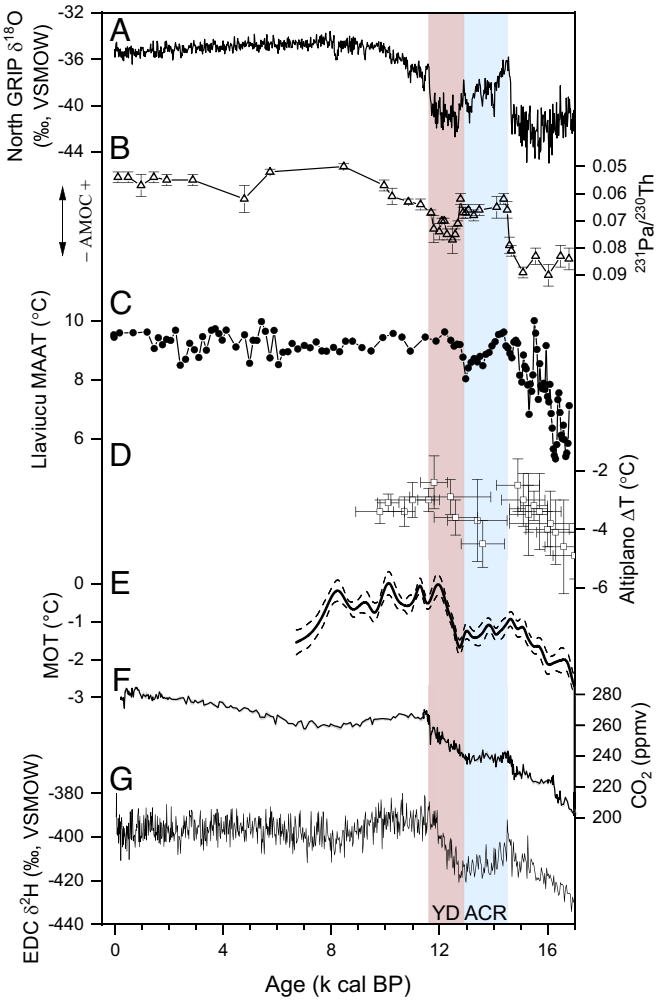

Fig. 3. Comparison of Llaviucu MAAT with other paleoclimatic records over the last deglaciation. (*A*) Greenland ice core (North GRIP) oxygen isotopes reflecting NH large-scale temperatures (61). (*B*) AMOC intensity based on $^{231}Pa/^{230}Th$ from marine sediment core (5). (*C*) brGDGT-based temperature reconstructions from Laguna Llaviucu, tropical South America. (*D*) Reconstructed Altiplano temperatures inferred from the paleoglacier and paleolake inversion framework (16). The values are expressed relative to the present MAT. (*E*) Mean global ocean temperature (MOT) derived from noble gas concentrations of air inclusions in ice cores (62). Dashed curves denote 1σ uncertainty. (*F*) Atmospheric CO_2 concentration (63). (*G*) Antarctica ice core (EPICA Dome C) hydrogen isotopes reflecting SH large-scale temperatures (59, 60). YD, Younger Dryas. ACR, Antarctic Cold Reversal.

Northern Hemisphere (NH) cooling and SH warming (2, 6). During the ACR, enhanced AMOC transported heat from the south to the north, leading to BA warming in the north and cooler SH sea surface temperatures (12). Recent study demonstrated that temperature changes are amplified over the continents (65), but the impacts of changes in high latitude temperatures and poleward heat transport by the ocean on tropical lands are unclear, particularly because atmospheric heat transport by the Hadley circulation partially compensates for the changes in heat transport by the AMOC (12, 66). The ACR has a potentially broader footprint as it is associated with a reduction in CO_2 outgassing from the Southern Ocean and a "pause" in the rise of atmospheric pCO_2 levels observed in ice cores (12, 67), which could explain its impacts on TSA temperatures. However, the pause in the rise of GHGs during the ACR only predicts a pause in the rate of warming, whereas our record indicates cooling during the ACR, similar to the cooling inferred from the combination of paleoglacier and paleolake records in the southern Tropical Andes (16) (Fig. 3 *C* and *D*). Although the mechanisms are not fully known, transient climate model experiments suggest cooling over much of TSA in response to high-latitude freshwater inputs, disruption of the AMOC, and increased northward ocean heat transport (11, 16). Our record is consistent with these model experiments (11), and supports the hypothesis that tropical Andean temperatures were mainly controlled both by atmospheric GHGs and variations in high latitude temperature and the AMOC.

Heterogeneous Tropical Land Temperatures Since the Deglaciation. A low-elevation land temperature reconstruction based on fluid inclusion microthermometry from tropical Asia shows slight cooling during the ACR (68) (Fig. 4), similar to our record. brGDGTs have been widely applied to African lake sediment records, but neither ACR nor YD cooling have been consistently detected in these data (69, 70) (Fig. 4). East Africa glacial recession was underway during the deglaciation, and glaciers were more extensive during the ACR than during the YD in some catchments, but the chronologies are not yet precise enough to link to millennial-scale events (71). Nevertheless, the cooling observed during the ACR in Laguna Llaviucu, alongside records from Andean glaciers and Southeast Asia, highlights the importance of ACR cooling in the tropics.

Holocene temperatures in Laguna Llaviucu are generally stable. This stands in contrast to temperature reconstructions from tropical Africa and higher latitudes, which show considerable warmth during the early to mid-Holocene relative to the late Holocene. This early to mid-Holocene warmth is not predicted from atmospheric pCO_2 concentrations, leading to the "Holocene temperature conundrum"— the contradiction between the global warming

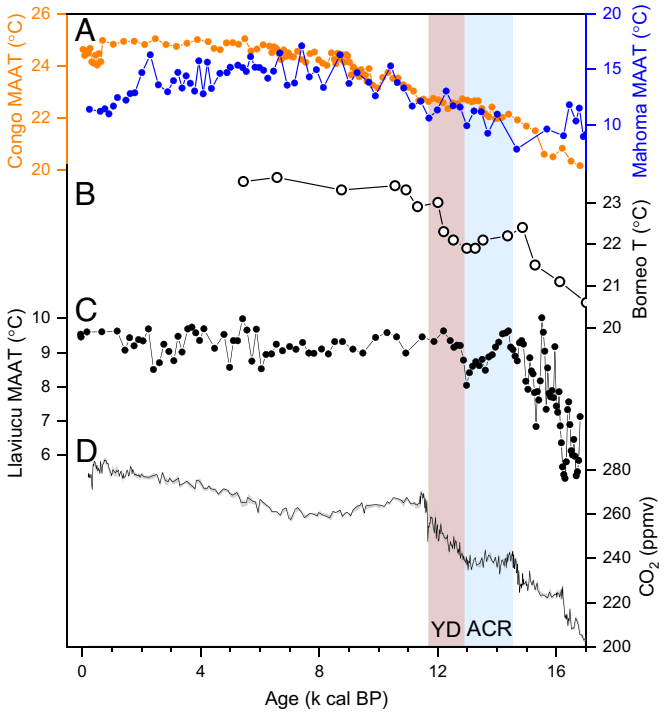

Fig. 4. Comparison of Llaviucu MAAT with other tropical temperature records and greenhouse gas forcing. (*A*) brGDGT-based temperature reconstructions from Africa. The orange line represents the Congo Basin temperature reconstruction (69). The blue line represents temperature reconstruction from Lake Mahoma, a high-elevation African lake (70). (*B*) Cave temperature record from tropical Asia based on stalagmite fluid inclusion microthermometry (68). (*C*) brGDGT-based temperature reconstructions from Laguna Llaviucu, tropical South America. (*D*) Atmospheric CO_2 concentration (63). YD, Younger Dryas. ACR, Antarctic Cold Reversal.

Downloaded from https://www.pnas.org by "BROWN UNIVERSITY , ROCKEFELLER LIBRARY" on May 23, 2025 from IP address 128.148.194.11.

simulated by climate models due to rising CO_2 versus the cooling trend during the mid to late-Holocene inferred from many proxy reconstructions (72, 73). Various hypotheses exist to resolve this conundrum, from land-surface albedo feedback (74) to seasonal biases in temperature proxies (75). Our results cannot reconcile the discrepancy between proxy records and climate model predictions; however, our recent brGDGT calibration work indicates that brGDGTs in the tropics are relatively insensitive to seasonal bias (33). The stability of temperatures and slight warming in our record during the Holocene are consistent with climate model simulations and suggest that TSA temperatures were influenced less strongly by land-surface feedback than in other parts of the world.

Overall, we find that CO_2 forcing, high latitude temperatures, and AMOC variability mainly govern tropical Andean temperature variations since the deglaciation. These factors affected other parts of the tropics, but our record also documents regional differences that highlight the importance of regional feedback and/or drivers of regional and global temperature changes.

Materials and Methods

Study Area. Laguna Llaviucu (Lake Llaviucu, 2°50′34″S, 79°8′43″W) lies within Cajas National Park, southern Ecuadorian Andes (*SI Appendix*, Fig. S1). This region was shaped by glaciers and contains hundreds of glacial lakes. Typically, bedrock is thick Quaternary silicic ignimbrite, rhyolite, and Tarqui formation (76). Laguna Llaviucu is an exorheic lake with an area of ~0.2 km^2 and a depth of 16.5 m. Water temperatures stays at ~12 °C until at least 12 m depths on June 3, 1988 (77). The upper ~11 m water column is oxygenated, and it is likely because of mixing by inflow and outflow (77).

Laguna Llaviucu lies on the eastern Andean flank where the climate is wet with mean annual precipitation exceeding 2,000 mm and a marked (June to September) dry season. The mean annual temperature is 11 to 12 °C and temperatures in the Cajas National Park show little seasonal variation other than diurnal changes.

Sediment Core Collection and Age-Depth Model. A 12.1-m sediment core (Llav09) from Laguna Llaviucu was collected using a Colinvaux-Vohnout piston sampler in June 2009. All tubes were capped and sealed in the field and then shipped to the Florida Institute of Technology. All cores were stored in a dark cold room (4 °C) until analysis.

To determine the chronology at Llaviucu, we used 14 radiocarbon (^{14}C) dates based on sediment bulk samples. A core, LLA-15, raised about 50 m southeast from Llav09 had a ^{210}Pb activity profile that showed a very slow sedimentation rate. We cross-correlated a distinctive peak of *Discostella* in the LLA-15 and Llav09 records at 2 cm depth (2.5 cm depth in the LLA-15 record) to allow us to adopt a ^{210}Pb activity profile for the uppermost 2 cm of this core (*SI Appendix*, Table S1). At 1,198 cm, a second correlation between a speleothem $\delta^{18}O$ record from Santiago cave and our *n*-alkane δ^2H record was used to constrain the age at the base of our age model. One ^{14}C dating reversal (OS-77396, depth 997, age 12,150 ± 50) was excluded to improve model fit. Calibration of ^{14}C ages used the IntCal20 calibration curve (78) and, together with the ^{210}Pb data and speleothem correlation, formed a chronology using "Bacon" in R (79, 80) with linear interpolations at the top of the core and a Bayesian age-depth model that incorporates uncertainties in both radiocarbon and model ages (*SI Appendix*, Fig. S3). The age-depth model has an average 1σ uncertainty of 154 ± 79, and the interval from 11.7 to 14.5 k cal BP has a 1σ uncertainty of 161 ± 53. To justify the robustness of this age-depth model, we tested the age-depth model with different calibrations (N. Hemisphere vs. S. Hemisphere) and different estimates of the basal age of the sediment core (*SI Appendix*, Fig. S7). We observed that the selection of using N. and S. Hemisphere calibrations (IntCal20 and SHCal20) has minimal effects on our records. The biggest impact on the age model comes from the choice of the tie-point at the base of the sediment succession. This impacts the timing of the onset of the millennial-scale cooling that we associate with the ACR by ~200 y but is insufficient to move the millennial-scale cooling to the start of the YD (*SI Appendix*, Fig. S7). Therefore, our age-depth model is adequate to determine the ages of millennial-scale events of YD and ACR.

Lipid Biomarker Analysis. A total of 121 samples were subsampled from the cores at every 10 cm with an average sampling resolution of ~60-y and ~200-y from 16.8 to 12.9 k cal BP, and 12.9 k cal BP to core-top, respectively. We freeze-dried and homogenized all samples, then acquired the total lipid extract (TLE) using a Dionex accelerated solvent extractor 350 with a solution of dichloromethane (DCM) and methanol (MeOH) (1:1, v/v). The TLE was further separated into apolar and polar fractions with alumina oxide column chromatography, and hexane/DCM (9:1, v/v) and DCM/MeOH (1:1, v/v) as mobile phases.

To measure leaf wax stable isotopes, we purified all apolar fractions with silver nitrate silica gel chromatography with hexane. The *n*-alkane concentrations were determined using a gas chromatograph equipped with a flame ionization detector. The concentrations were used to calculate suitable dilutions for isotope measurements aiming for a ~4.5 V peak intensity. The δ^2H of C_{31} *n*-alkane for a total of 121 samples was measured on a Thermo Delta V Advantage isotope ratio mass spectrometer coupled to a Thermo Trace 1310 GC through a ConFlo IV. The $\delta^{13}C$ of C_{31} *n*-alkane for a total of 25 samples was measured on a Thermo Delta V Advantage isotope ratio mass spectrometer coupled to an Agilent 6890 GC through a Finnigan GCC III. All samples were measured in triplicate, bracketed by three injections of reference gas, with laboratory standards injections between each sample to track and correct intersample drift. Sample δ^2H ratios are shown in per mil (‰) relative to Vienna Standard Mean Ocean Water (VSMOW). Sample $\delta^{13}C$ ratios are shown in per mil (‰) relative to Vienna Peedee Belemnite (VPDB).

To measure brGDGTs, we dissolved all polar fractions in hexane/isopropanol (99:1, v/v), and filtered the samples through 0.45-μm PTFE syringe filters. Then we analyzed all filtered samples on an Agilent 1200 series HPLC coupled to an Agilent 6130 quadrupole mass selective detector following the method (81) that can differentiate the 5- and 6-methyl brGDGT isomers. Selected ion monitoring mode was used to scan for mass/charge ratios of 1,302, 1,300, 1,298, 1,296, 1,292, 1,050, 1,048, 1,046, 1,036, 1,034, 1,032, 1,022, 1,020, and 1,018. We used the previously established MBT'_{5ME} (methylation of 5-methyl branched tetraethers) index (31, 32) and newly developed pantropical temperature calibration (33) to reconstruct temperatures from Laguna Llaviucu:

$$MBT'_{5ME} = (Ia + Ib + Ic)/(Ia + Ib + Ic + IIa + IIb + IIc + IIIa), \quad [1]$$

$$MAAT = -1.78 + 31.01 \times MBT'_{5ME}. \quad [2]$$

This calibration has a RMS error of 2.26 °C (33).

Temperature Reconstruction Based on brGDGTs. brGDGTs contain alkyl core chains with four to six methyl groups and zero to two cyclopentyl moieties (31, 82, 83). These compounds are ubiquitous in a wide range of terrestrial environments (84). Although the organisms responsible for brGDGTs production in lakes remain unknown, recent research points to production by Acidobacteria (85–87). When the ambient temperature changes, the brGDGT producers could alter their lipid membranes' composition to maintain appropriate fluidity and permeability. Therefore, fossil brGDGTs can be used to reconstruct past temperatures.

Our recent calibration work shows a unified response between brGDGT to MAAT from the pantropical regions (33). Specifically, the new brGDGT dataset from tropical South America validates the application of lacustrine brGDGTs in paleotemperature reconstruction in this region (33). In addition to the MBT'_{5ME} calibration (Eq. **2**), we also test the multivariate linear regression (MLR) calibration (33)

$$MAAT = -4.11 + 31.63 \times f(Ia) + 64.50 \times f(Ib) + 32.28 \times f(IIa'). \quad [3]$$

Both reconstructions show almost identical structures and both surface datapoints are close to the observed MAAT value (*SI Appendix*, Fig. S8). Given the MLR model is thought to be lacking a well-defined underlying biophysiological mechanism, whereas the correlation between MBT'_{5ME} and temperature has been found in culture studies (86), we report our temperature based on the MBT'_{5ME} calibration but argue this similar structure further improve the creditableness of using brGDGTs to reconstruct temperatures from Laguna Llaviucu.

Downloaded from https://www.pnas.org by "BROWN UNIVERSITY , ROCKEFELLER LIBRARY" on May 23, 2025 from IP address 128.148.194.11.

Hydroclimate Reconstruction Based on δ^2H of C_{31} *n*-Alkane. *n*-Alkanes, saturated unbranched acyclic hydrocarbons with the chemical formula C_nH_{2n+2}, form the waxy surface of plant leaves. The *n*-alkanes with long-chain length are mainly synthesized by terrestrial plants as a coating to protect from water loss (88). The *n*-alkanes are primarily sourced from the plant's source water. Therefore, δ^2H of fossil *n*-alkanes can be used to infer the source water's isotope signatures in the past (89).

This proof of concept is further tested by Feakins et al. (37). In the Andes and Amazon, δ^2H of plant *n*-alkanes have been found strongly correlated with the time-averaged precipitation's hydrogen isotopes (37). Furthermore, based on Global Network of Isotopes in Precipitation (GNIP) data from the closest station (CUENCA, 2°52′59.99″S, 78°58′59.99″W, *SI Appendix*, Fig. S1), δ^2H of precipitation is significantly negatively correlated with the amount of precipitation (*SI Appendix*, Fig. S2). Taken together, more depleted (enriched) δ^2H values of *n*-alkanes represent more (less) precipitations.

Fornace et al. (34) generated a C_{28} *n*-alkanoic acid hydrogen isotope record from Lake Titicaca, Central Andes, to reconstruct hydrologic variability. Their record generally tracks other stalagmite oxygen isotopes, supporting the notion of using sedimentary leaf wax δ^2H to infer past hydroclimate in this region (34). Here, we report δ^2H of C_{31} *n*-alkanes as the indicator of hydroclimate and note modern observational data support the use of *n*-alkanes over the *n*-alkanoic acids as the proxy to reconstruct hydroclimate variability (37).

Significant Correlation between Llaviucu δ^2H and Santiago Cave $\delta^{18}O$ Records. Our δ^2H record has a ~200-y resolution from 12.9 k cal BP to core-top, and ~60-y resolution from the bottom to 12.9 k cal BP, whereas the Santiago cave record has a resolution of ~50-y and ~70-y during those two intervals. To calculate the correlation between these records, we interpolated both records at 10-y resolution and then calculated bin averages to acquire 200-y resolution records from 12.9 to 6.3 k cal BP ($N = 34$) and 100-y records from 16.8 to 12.9 k cal BP ($N = 39$). Following this resampling the two records are significantly correlated (Fig. 2*B*). It is worth noting that both records have different dating methods, further suggesting our Llaviucu records' chronology is sufficiently accurate to document the timing of millennial-scale climate events in this region.

Data, Materials, and Software Availability. All study data are included in the article and/or supporting information. Time series data have been deposited in NOAA NCEI Paleoclimatology Archive (https://www.ncei.noaa.gov/access/paleo-search/study/39579).

ACKNOWLEDGMENTS. We thank the Editor and three anonymous reviewers for their constructive comments that helped improve this paper. This work was supported by U.S. NSF (DEB-2029614 award to J.M.R.; DEB-2029649 award to M.B.B.)

Author affiliations: [a]Department of Earth, Environmental, and Planetary Sciences, Brown University, Providence, RI 02912; [b]Institute for Global Ecology, Florida Institute of Technology, Melbourne, FL 32901; and [c]Department of Ecosystem and Landscape Dynamics, Institute for Biodiversity and Ecosystem Dynamics, University of Amsterdam, Amsterdam 1098 XH, The Netherlands

1. P. U. Clark *et al.*, Global climate evolution during the last deglaciation. *Proc. Natl. Acad. Sci. U.S.A.* **109**, E1134–E1142 (2012).
2. J. D. Shakun *et al.*, Global warming preceded by increasing carbon dioxide concentrations during the last deglaciation. *Nature* **484**, 49–54 (2012).
3. T. Blunier *et al.*, Asynchrony of Antarctic and Greenland climate change during the last glacial period. *Nature* **394**, 739–743 (1998).
4. R. Seager, D. S. Battisti, "Challenges to our understanding of the general circulation" in *The Global Circulation of the Atmosphere* (Princeton University Press, 2007), pp. 331–372.
5. J. F. McManus, R. Francois, J. M. Gherardl, L. Kelgwin, S. Drown-Leger, Collapse and rapid resumption of Atlantic meridional circulation linked to deglacial climate changes. *Nature* **428**, 834–837 (2004).
6. Z. Liu *et al.*, Transient simulation of last deglaciation with a new mechanism for Bølling-Allerød warming. *Science* 325, 310–314 (2009).
7. S. E. Loomis *et al.*, The tropical lapse rate steepened during the Last Glacial Maximum. *Sci. Adv.* **3**, 1–8 (2017).
8. L. A. Powers *et al.*, Large temperature variability in the southern African tropics since the Last Glacial Maximum. *Geophys. Res. Lett.* **32**, 1–4 (2005).
9. J. E. Tierney *et al.*, Northern hemisphere controls on tropical Southeast African climate during the past 60,000 years. *Science* 322, 252–255 (2008).
10. S. E. Loomis, J. M. Russell, B. Ladd, F. A. Street-Perrott, J. S. Sinninghe Damsté, Calibration and application of the branched GDGT temperature proxy on East African lake sediments. *Earth Planet. Sci. Lett.* **357–358**, 277–288 (2012).
11. V. Jomelli *et al.*, A major advance of tropical Andean glaciers during the Antarctic cold reversal. *Nature* **513**, 224–228 (2014).
12. J. B. Pedro *et al.*, The spatial extent and dynamics of the Antarctic Cold Reversal. *Nat. Geosci.* **9**, 51–55 (2016).
13. T. Van Der Hammen, H. Hooghiemstra, The EL abra stadial, a younger dryas equivalent in Colombia. *Q. Sci. Rev.* **14**, 841–851 (1995).
14. R. Van'T Veer, G. A. Islebe, H. Hooghiemstra, Climatic change during the Younger Dryas chron in northern South America A test of the evidence. *Q. Sci. Rev.* **19**, 1821–1835 (2000).
15. D. T. Rodbell, J. A. Smith, B. G. Mark, Glaciation in the Andes during the Lateglacial and Holocene. *Q. Sci. Rev.* **28**, 2165–2212 (2009).
16. L. C. P. Martin *et al.*, Antarctic-like temperature variations in the Tropical Andes recorded by glaciers and lakes during the last deglaciation. *Q. Sci. Rev.* **247**, 106542 (2020).
17. D. Palacios *et al.*, The deglaciation of the Americas during the Last Glacial Termination. *Earth-Sci. Rev.* **203**, 103113 (2020).
18. B. G. Mark *et al.*, Tropical snowline changes at the last glacial maximum: A global assessment. *Q. Int.* **138–139**, 168–201 (2005).
19. C. Kull, S. Imhof, M. Grosjean, R. Zech, H. Veit, Late Pleistocene glaciation in the Central Andes: Temperature versus humidity control–A case study from the eastern Bolivian Andes (17°S) and regional synthesis. *Global Planet. Change* **60**, 148–164 (2008).
20. M. Stute *et al.*, Cooling of tropical Brazil (5°C) during the last glacial maximum. *Science* 269, 379–383 (1995).
21. M. H. M. Groot *et al.*, Ultra-high resolution pollen record from the northern Andes reveals rapid shifts in montane climates within the last two glacial cycles. *Clim. Past* **7**, 299–316 (2011).
22. M. F. Raczka *et al.*, A human role in Andean megafaunal extinction? *Q. Sci. Rev.* **205**, 154–165 (2019).
23. P.-H. Blard *et al.*, Late local glacial maximum in the Central Altiplano triggered by cold and locally-wet conditions during the paleolake Tauca episode (17–15ka, Heinrich 1). *Q. Sci. Rev.* **28**, 3414–3427 (2009).
24. J. D. Shakun *et al.*, Cosmogenic dating of Late Pleistocene glaciation, southern tropical Andes, Peru. *J. Q. Sci.* **30**, 841–847 (2015).
25. G. Balco, J. O. Stone, N. A. Lifton, T. J. Dunai, A complete and easily accessible means of calculating surface exposure ages or erosion rates from 10Be and 26Al measurements. *Q. Geochronol.* **3**, 174–195 (2008).
26. L. C. P. Martin *et al.*, The CREp program and the ICE-D production rate calibration database: A fully parameterizable and updated online tool to compute cosmic-ray exposure ages. *Q. Geochronol.* **38**, 25–49 (2017).
27. P.-H. Blard, R. Braucher, J. Lavé, D. Bourlès, Cosmogenic 10Be production rate calibrated against 3He in the high Tropical Andes (3800–4900 m, 20–22° S). *Earth Planet. Sci. Lett.* **382**, 140–149 (2013).
28. P.-H. Blard *et al.*, Cosmogenic 3He production rate in the high tropical Andes (3800 m, 20°S): Implications for the local last glacial maximum. *Earth Planet. Sci. Lett.* **377–378**, 260–275 (2013).
29. M. A. Kelly *et al.*, A locally calibrated, late glacial 10 Be production rate from a low-latitude, high-altitude site in the Peruvian Andes. *Q. Geochronol.* **26**, 70–85 (2015).
30. L. C. P. Martin *et al.*, In situ cosmogenic 10Be production rate in the High Tropical Andes. *Q. Geochronol.* **30**, 54–68 (2015).
31. C. De Jonge *et al.*, Occurrence and abundance of 6-methyl branched glycerol dialkyl glycerol tetraethers in soils: Implications for palaeoclimate reconstruction. *Geochim. Cosmochim. Acta* **141**, 97–112 (2014).
32. J. M. Russell, E. C. Hopmans, S. E. Loomis, J. Liang, J. S. Sinninghe Damsté, Distributions of 5- and 6-methyl branched glycerol dialkyl glycerol tetraethers (brGDGTs) in East African lake sediment: Effects of temperature, pH, and new lacustrine paleotemperature calibrations. *Org. Geochem.* **117**, 56–69 (2018).
33. B. Zhao *et al.*, Evaluating global temperature calibrations for lacustrine branched GDGTs: Seasonal variability, paleoclimate implications, and future directions. *Q. Sci. Rev.* **310**, 108124 (2023).
34. K. L. Fornace *et al.*, A 60,000-year record of hydrologic variability in the Central Andes from the hydrogen isotopic composition of leaf waxes in Lake Titicaca sediments. *Earth Planet. Sci. Lett.* **408**, 263–271 (2014).
35. M. Vuille, M. Werner, Stable isotopes in precipitation recording South American summer monsoon and ENSO variability: Observations and model results. *Clim. Dyn.* **25**, 401–413 (2005).
36. W. Dansgaard, Stable isotopes in precipitation. *Tellus* **16**, 436–468 (1964).
37. S. J. Feakins *et al.*, Plant leaf wax biomarkers capture gradients in hydrogen isotopes of precipitation from the Andes and Amazon. *Geochim. Cosmochim. Acta* **182**, 155–172 (2016).
38. B. L. Konecky, D. C. Noone, K. M. Cobb, The influence of competing hydroclimate processes on stable isotope ratios in tropical rainfall. *Geophys. Res. Lett.* **46**, 1622–1633 (2019).
39. S. E. Fick, R. J. Hijmans, WorldClim 2: New 1-km spatial resolution climate surfaces for global land areas. *Int. J. Climatol.* **37**, 4302–4315 (2017).
40. N. A. S. Mosblech *et al.*, North Atlantic forcing of Amazonian precipitation during the last ice age. *Nat. Geosci.* **5**, 817–820 (2012).
41. J. Laskar *et al.*, A long-term numerical solution for the insolation quantities of the Earth. *Astron. Astrophys.* **428**, 261–285 (2004).
42. F. W. Cruz *et al.*, Insolation-driven changes in atmospheric circulation over the past 116,000 years in subtropical Brazil. *Nature* **434**, 63–66 (2005).
43. H. Cheng *et al.*, Climate change patterns in Amazonia and biodiversity. *Nat. Commun.* **4**, 1411 (2013).
44. P. A. Baker *et al.*, The history of South American tropical precipitation for the past 25,000 years. *Science* 291, 640–643 (2001).
45. P. A. Baker *et al.*, Tropical climate changes at millennial and orbital timescales on the bolivian Altiplano. *Nature* **409**, 698–701 (2001).
46. A. Woods *et al.*, Andean drought and glacial retreat tied to Greenland warming during the last glacial period. *Nat. Commun.* **11**, 1–7 (2020).
47. D. T. Rodbell *et al.*, 700,000 years of tropical Andean glaciation. *Nature* **607**, 301–306 (2022).

Downloaded from https://www.pnas.org by "BROWN UNIVERSITY , ROCKEFELLER LIBRARY" on May 23, 2025 from IP address 128.148.194.11.

48. G. H. Haug, K. A. Hughen, D. M. Sigman, L. C. Peterson, U. Röhl, Southward migration of the intertropical convergence zone through the holocene. *Science* 293, 1304–1308 (2001).
49. C. M. Moy, G. O. Seltzer, D. T. Rodbell, D. M. Anderson, Variability of El Niño/Southern Oscillation activity at millennial timescales during the Holocene epoch. *Nature* **420**, 162–165 (2002).
50. K. Hagemans *et al.*, Intensification of ENSO frequency drives forest disturbance in the Andes during the Holocene. *Q. Sci. Rev.* **294**, 107762 (2022).
51. K. Hagemans *et al.*, Patterns of alluvial deposition in Andean lake consistent with ENSO trigger. *Q. Sci. Rev.* **259**, 106900 (2021).
52. S. Z. Mark, M. B. Abbott, D. T. Rodbell, C. M. Moy, XRF analysis of Laguna Pallcacocha sediments yields new insights into Holocene El Niño development. *Earth Planet. Sci. Lett.* **593**, 117657 (2022).
53. M. N. Nascimento *et al.*, The adoption of agropastoralism and increased ENSO frequency in the Andes. *Q. Sci. Rev.* **243**, 106471 (2020).
54. T. Schneider, H. Hampel, P. V. Mosquera, W. Tylmann, M. Grosjean, Paleo-ENSO revisited: Ecuadorian Lake Pallcacocha does not reveal a conclusive El Niño signal. *Global Planet. Change* **168**, 54–66 (2018).
55. J. Kiefer, C. Karamperidou, High-resolution modeling of ENSO-induced precipitation in the Tropical Andes: Implications for proxy interpretation. *Paleoceanogr. Paleoclimatol.* **34**, 217–236 (2019).
56. M. C. Parish, X. Du, S. Bijaksana, J. M. Russell, A brGDGT-based reconstruction of terrestrial temperature from the maritime continent spanning the last glacial maximum. *Paleoceanogr. Paleoclimatol.* **38**, 1–17 (2023).
57. A. J. Baxter *et al.*, Reversed Holocene temperature–moisture relationship in the Horn of Africa. *Nature* **620**, 336–343 (2023).
58. M. B. Bush, M. R. Silman, D. H. Urrego, 48,000 years of climate and forest change in a biodiversity hot spot. *Science* 303, 827–829 (2004).
59. J. Jouzel *et al.*, Orbital and millennial Antarctic climate variability over the past 800,000 years. *Science* 317, 793–796 (2007).
60. B. Lemieux-Dudon *et al.*, Consistent dating for Antarctic and Greenland ice cores. *Q. Sci. Rev.* **29**, 8–20 (2010).
61. K. K. Andersen *et al.*, High-resolution record of Northern Hemisphere climate extending into the last interglacial period. *Nature* **431**, 147–151 (2004).
62. B. Bereiter, S. Shackleton, D. Baggenstos, K. Kawamura, J. Severinghaus, Mean global ocean temperatures during the last glacial transition. *Nature* **553**, 39–44 (2018).
63. B. Bereiter *et al.*, Revision of the EPICA Dome C CO_2 record from 800 to 600 kyr before present. *Geophys. Res. Lett.* **42**, 542–549 (2015).
64. F. Parrenin *et al.*, Synchronous change of atmospheric CO_2 and Antarctic temperature during the last deglacial warming. *Science* 339, 1060–1063 (2013).
65. A. M. Seltzer, P. H. Blard, S. C. Sherwood, M. Kageyama, Terrestrial amplification of past, present, and future climate change. *Sci. Adv.* **9**, 1–9 (2023).
66. C. Wunsch, Abrupt climate change: An alternative view. *Q. Res.* **65**, 191–203 (2006).
67. M. S. Fletcher *et al.*, Northward shift of the southern westerlies during the Antarctic Cold Reversal. *Q. Sci. Rev.* **271**, 107189 (2021).
68. M. H. Løland *et al.*, Evolution of tropical land temperature across the last glacial termination. *Nat. Commun.* **13**, 5158 (2022).
69. J. W. H. Weijers, E. Schefuß, S. Schouten, J. S. S. Damsté, Coupled thermal and hydrological evolution of tropical Africa over the last deglaciation. *Science* 315, 1701–1704 (2007).
70. S. Garelick *et al.*, The dynamics of warming during the last deglaciation in high-elevation regions of Eastern Equatorial Africa. *Q. Sci. Rev.* **281**, 107416 (2022).
71. M. S. Jackson *et al.*, Glacial fluctuations in tropical Africa during the last glacial termination and implications for tropical climate following the Last Glacial Maximum. *Q. Sci. Rev.* **243**, 106455 (2020).
72. Z. Liu *et al.*, The Holocene temperature conundrum. *Proc. Natl. Acad. Sci. U.S.A.* **111** E3501–E3505 (2014).
73. D. S. Kaufman, E. Broadman, Revisiting the Holocene global temperature conundrum. *Nature* **614**, 425–435 (2023).
74. A. J. Thompson, J. Zhu, C. J. Poulsen, J. E. Tierney, C. B. Skinner, Northern Hemisphere vegetation change drives a Holocene thermal maximum. *Sci. Adv.* **8**, 1–11 (2022).
75. S. Bova, Y. Rosenthal, Z. Liu, S. P. Godad, M. Yan, Seasonal origin of the thermal maxima at the Holocene and the last interglacial. *Nature* **589**, 548–553 (2021).
76. D. T. Rodbell, S. Bagnato, J. C. Nebolini, G. O. Seltzer, M. B. Abbott, A Late Glacial-Holocene Tephrochronology for glacial lakes in Southern Ecuador. *Q. Res.* **57**, 343–354 (2002).
77. P. A. Colinvaux, M. B. Bush, M. Steinitz-Kannan, M. C. Miller, Glacial and postglacial pollen records from the Ecuadorian Andes and Amazon. *Q. Res.* **48**, 69–78 (1997).
78. P. J. Reimer *et al.*, The IntCal20 Northern Hemisphere radiocarbon age calibration curve (0–55 cal kBP). *Radiocarbon* **62**, 725–757 (2020).
79. M. Blaauw, Methods and code for 'classical' age-modelling of radiocarbon sequences. *Q. Geochronol.* **5**, 512–518 (2010).
80. M. Blaauw, J. A. Christen, Flexible paleoclimate age-depth models using an autoregressive gamma process. *Bayesian Anal.* **6**, 457–474 (2011).
81. E. C. Hopmans, S. Schouten, J. S. Sinninghe Damsté, The effect of improved chromatography on GDGT-based palaeoproxies. *Org. Geochem.* **93**, 1–6 (2016).
82. J. W. H. Weijers, S. Schouten, J. C. van den Donker, E. C. Hopmans, J. S. Sinninghe Damsté, Environmental controls on bacterial tetraether membrane lipid distribution in soils. *Geochim. Cosmochim. Acta* **71**, 703–713 (2007).
83. J. S. Sinninghe Damsté, E. C. Hopmans, R. D. Pancost, S. Schouten, J. A. J. Geenevasen, Newly discovered non-isoprenoid glycerol dialkyl glycerol tetraether lipids in sediments. *Chem. Commun.* **2000**, 1683–1684 (2000).
84. S. Schouten, E. C. Hopmans, J. S. Sinninghe Damsté, The organic geochemistry of glycerol dialkyl glycerol tetraether lipids: A review. *Org. Geochem.* **54**, 19–61 (2013).
85. J. S. Sinninghe Damsté *et al.*, An overview of the occurrence of ether- and ester-linked iso-diabolic acid membrane lipids in microbial cultures of the Acidobacteria: Implications for brGDGT paleoproxies for temperature and pH. *Org. Geochem.* **124**, 63–76 (2018).
86. Y. Chen *et al.*, The production of diverse brGDGTs by an Acidobacterium providing a physiological basis for paleoclimate proxies. *Geochim. Cosmochim. Acta* **337**, 155–165 (2022), https://doi.org/10.1016/j.gca.2022.08.033.
87. T. A. Halamka *et al.*, Production of diverse brGDGTs by Acidobacterium Solibacter usitatus in response to temperature, pH, and O_2 provides a culturing perspective on brGDGT proxies and biosynthesis. *Geobiology* **21**, 102–118 (2023).
88. G. Eglinton, R. J. Hamilton, Leaf epicuticular waxes. *Science* 156, 1322–1335 (1967).
89. D. Sachse *et al.*, Molecular Paleohydrology: Interpreting the hydrogen-isotopic composition of lipid biomarkers from photosynthesizing organisms. *Annu. Rev. Earth Planet. Sci.* **40**, 221–249 (2012).

Downloaded from https://www.pnas.org by "BROWN UNIVERSITY , ROCKEFELLER LIBRARY" on May 23, 2025 from IP address 128.148.194.11.